### Title

Evaluation of thermo-mechanical and thermal behavior of full-scale energy foundations




### Journal

Acta Geotechnica, 10(2)

### ISSN

1861-1125



### Authors

Murphy, Kyle D
McCartney, John S
Henry, Karen S



### Publication Date

2015-04-01

### DOI

10.1007/s11440-013-0298-4

Peer reviewed

# Evaluation of Thermo-Mechanical and Thermal Behavior of Full-Scale Energy Foundations

Kyle D. Murphy[1], John S. McCartney[2], and Karen S. Henry[3]

[1]Graduate Research Assistant, University of Colorado Boulder, Dept. of Civil, Env. and Arch. Engineering, UCB 428, Boulder, CO 80309, kyle.murphy@colorado.edu

[2]Associate Professor and Lyall Faculty Fellow, University of Colorado Boulder, Dept. of Civil, Env. and Arch. Engineering, UCB 428, Boulder, CO 80309, john.mccartney@colorado.edu

[3]Associate Professor, United States Air Force Academy, Department of Civil Engineering, USAF Academy, CO 80840-6232, karen.henry@usafa.edu

## Abstract

Eight full-scale energy foundations were constructed for a new building at the U.S. Air Force Academy (USAFA). The foundations are being used to demonstrate this technology to the United States Department of Defense, and have several experimental features in order to study of their thermal-mechanical behavior. Three of the foundations are instrumented with strain gages and thermistors, and their thermo-mechanical response during a heating and cooling test were evaluated. For a temperature increase of 18°C, the maximum thermal axial stress ranged from 4.0 to 5.1 MPa, which is approximately 25% of the compressive strength of concrete (estimated at 21 MPa) and the maximum upward displacement ranged from 1.4 to 1.7 mm, which should not cause angular distortions sufficient enough to cause structural or aesthetic damage of the building. The end restraint provided by the building was observed to change depending on the location of the foundation. The heat flux per meter was measured by evaluating the temperatures and flow rates of a heat exchanger fluid entering and exiting the foundations. The heat flux values were consistent with those in the literature, and the foundation with the 3 continuous heat exchanger loops was found to have the greatest heat flux per meter. The transient thermal conductivity of the subsurface measured using the temperatures of the subsurface surrounding the foundation ranged from 2.0 to 2.3 W/mK, which is consistent with results from thermal response tests on energy foundations reported in the literature.

Keywords: Geothermal Heat Exchange, Deep Foundations, Thermo-Mechanical Behavior; Thermal Response Test

# 1 Introduction

Heating and cooling of buildings comprises nearly 50% of the total building energy usage in the United States (Energy Information Administration 2008). Ground-source heat exchange (GSHE) systems are an approach to reduce the energy demand of heating and cooling systems compared to conventional air-source heat pump systems. The most common GSHE system involves the use of a closed loop heat exchanger to transfer heat between the subsurface soil or rock and an overlying structure, taking advantage of the relatively constant natural ground temperature below the depth of seasonal variation (Brandl 2006). The subsurface below a depth of 4 m generally has a relatively constant temperature approximately equal to the mean annual air temperature at a given location, and thus permits the efficiency of a ground-source heat exchange system to be higher than that of an air-source heat exchange system (Kavanaugh et al. 1997).

Although conventional ground-source heat exchange (GSHE) systems have been used for many years, the additional cost of drilling deep boreholes for the sole purpose of exchanging heat with the ground has rendered this technology cost-prohibitive in some situations (Hughes 2008). Energy foundations are a feasible approach to enhance implementation of GSHE systems by reducing installation costs through taking advantage of initial construction activities (Brandl 2006; Adam and Markiewicz 2009). In this study, energy foundations refer to drilled shaft foundations constructed with a set of closed-loop heat exchangers attached to the inside of the reinforcement cage so that they can serve the dual purposes of providing structural support and providing access to ground thermal energy. While energy foundations are gaining popularity throughout the world, further research is required to fully understand their performance in terms of thermal response and thermo-mechanical behavior in different soil profiles. This paper focuses on the characterization of a series of eight energy foundations installed in an unsaturated sandstone deposit.

# 2 Background

## 2.1 Thermo-mechanical Behavior

As a deep foundation is loaded mechanically, the axial stress is expected to be highest at the head and decrease with depth as side shear resistance is mobilized at the soil-foundation interface. The axial stress will decrease to zero if the side shear resistance is sufficient to support the building load; if not, it will decrease to a non-zero value and there will be end bearing resistance in the material underlying the toe of the foundation. As an energy foundation is heated or cooled, the reinforced concrete will tend to expand or contract axially about a point referred to as the “null point” (Knellwolf et al. 2011). The null point is the point of zero axial displacement during heating or cooling, and its location depends on the stiffness of the end boundaries imposed by the overlying superstructure and the material beneath the toe, as well as the distribution of mobilized side shear resistance (Bourne-Webb et al. 2009; Amatya et al. 2012). It

is also likely that radial expansion of the foundation will occur as the foundation is heated (Laloui et al. 2006), which may result in a net increase in ultimate side shear resistance (McCartney and Rosenberg 2011; Ouyang et al. 2011).

The upper limit on the thermal axial strain $\varepsilon_T$ in an energy foundation is the free expansion (i.e., unrestrained) thermal axial strain $\varepsilon_{T,free}$, defined as follows:

$$\varepsilon_{T,free} = \alpha_c \Delta T \quad \textbf{(1)}$$

where $\alpha_c$ is the coefficient of linear thermal expansion of reinforced concrete and $\Delta T$ is the change in temperature. For geotechnical engineering purposes, the thermal axial strain is defined as positive during compression. Accordingly, $\alpha_c$ is defined as negative because structural elements expand during heating (i.e., positive $\Delta T$). For the case that an energy foundation is restrained from moving such that the actual thermal axial strain $\varepsilon_T$ is less than that predicted by Equation 1, the thermal axial stresses $\sigma_T$ can be calculated as follows:

$$\sigma_T = E(\varepsilon_T - \alpha_c \Delta T) \quad \textbf{(2)}$$

where E is the Young's modulus of reinforced concrete. For energy foundations, soil-structure interaction mechanisms will restrict the movement of the foundation during heating. The side shear resistance, end bearing, and building restraint will influence the distribution in thermally induced stresses and strains (Mimouni and Laloui 2013). Soil-structure interaction mechanisms of energy foundations have been studied in centrifuge-scale tests for simplified soil profiles (McCartney and Rosenberg 2011; Stewart and McCartney 2014). However, evaluation of full-scale foundations imposes a set of real boundary conditions and soil strata. Several full-scale energy foundations have been evaluated to study the thermo-mechanical stresses and strains during mechanical loading, heating, and cooling (Laloui et al. 2006; Bourne-Webb et al. 2009; Amatya et al. 2012; McCartney and Murphy 2012) (Table 1). The thermal axial stress ranges from -1 to 5MPa and the thermal axial displacement of the foundation head ranges from -4.2 mm upward to +4.0 downward. The axial stresses are well within the compressive strength of reinforced concrete, and the axial displacements of the foundation would not lead to significant angular distortions to cause architectural damage for most buildings.

## 2.2 Thermal Behavior

The thermal behavior of energy foundations depends on many factors including the thermal properties of individual materials in the GSHE, site stratigraphy, groundwater and its flow, heat exchanger configuration within foundation and dimensions of the energy foundation, and thermal demands of the building (Brandl 2006). To optimize the design of GSHE, the system thermal conductivity, specific heat capacity, borehole resistance, and heat exchange rate must be evaluated accurately (Sanner 2001). For the purposes of this study, the primary mode of heat transport in the soil surrounding energy foundations is assumed to be by conduction. There is little to no groundwater present in the soil profile of the foundation installations, hence

105 groundwater flow (and convective heat transfer) is considered to be negligible. The heat flux
106 from a cylindrical source (i.e., an energy foundation) is given by:

$$Q = -2\pi R l \lambda \frac{dT}{dr} \quad \textbf{(3)}$$

107 where $Q$ is the heat flux in Watts being supplied to the energy foundation, R is the radius of the
108 energy foundation, $l$ is the length of the energy foundation, λ is the thermal conductivity of the
109 medium in contact with the cylindrical source, and dT/dr is the temperature gradient in the radial
110 direction. Convection is the main heat flow process in the fluid itself as the fluid flow rate is
111 sufficient to lead to a turbulent flow pattern, while conduction is dominant through the heat
112 exchanger pipe, concrete, and into the ground. As it is difficult to measure the thermal properties
113 of the individual soil layers and materials in energy foundations, they are typically characterized
114 using a system value.

115 Thermal response tests (TRT) are the most common method of determining thermal
116 properties of the subsurface and energy foundation system (Brandl 2006). Thermal response
117 testing of geothermal borehole heat exchangers has been in use for several years (Sanner et al.
118 2005), and involves circulating a fluid through a heat exchanger while supplying a constant
119 amount of power to the fluid. During a TRT the temperatures of the fluid entering and exiting the
120 foundation are monitored over a period of several days. The measured values of the fluid supply
121 and return temperatures and the mass flow rate through each foundation can be used to calculate
122 the input heat flux, as follows:

$$Q = \Delta T \dot{V} \rho_{fluid} C_{fluid} \quad \textbf{(4)}$$

123 where ΔT is the difference between the supply and return fluid temperatures in K ($T_{supply}$ and
124 $T_{return}$, respectively), $\dot{V}$ is the fluid flow rate in $m^3/s$, $\rho_{fluid}$ is the mass density of the fluid $kg/m^3$,
125 and $C_{fluid}$ is the specific heat capacity of the fluid in J/(kgK). The heat flux density can be
126 calculated by dividing Equation (4) by the cross-sectional area of the heat exchanger tubing.

127 Several studies have used the simple analytical solutions to investigate the thermal behavior
128 of full-scale energy foundations in different soil types with various heat exchanger loop
129 configurations and foundation geometries (Hamada et al. 2007; Ooka 2007; Gao 2008; Lennon et
130 al. 2009; Brettmann and Amis 2011). The results of these studies are summarized in Table 2. The
131 system thermal conductivity values reported in these studies ranges from 2.4 to 6.0 W/mK,
132 which is much higher than the thermal conductivity of most geological and structural materials,
133 suggesting that the thermal conductivity values may incorporate the effects of the heat capacity
134 of the concrete and may not represent steady-state conditions (Loveridge and Powrie 2012). In
135 these studies, the TRT was performed at the head of the foundation before the building has been
136 constructed. However, there has not been a thorough evaluation of TRT results on foundations
137 after construction and plumbing is complete. The fact that the tubing used to connect the energy
138 foundation to the heat pump is often not insulated for practical construction purposes means that

the heat exchange response of the energy foundation system may be affected by ambient surface fluctuations.

# 3 Project Description

## 3.1 Building Description

A one-story, shower-shave building was constructed at the Field Engineering and Readiness Laboratory (FERL) of the US Air Force Academy (USAFA) beginning March, 2012. The building provides restrooms, showers, and laundry facilities for 100 people. The building will also be used to evaluate the performance of energy efficient technologies to aid in the development of "net zero" energy consuming structures for the U.S. Department of Defense (DoD). These technologies include energy foundations, a radiant in-floor heating system, solar photovoltaic panels, and a solar water heating system. Each component will be continuously monitored to evaluate the energy usage or output of each technology. In addition to the ground-source heat pump coupled with the energy foundations, the building contains a natural gas boiler heating system. Having both conventional and ground-source HVAC systems permits comparison of their energy efficiencies under similar environmental conditions.

## 3.2 Subsurface Conditions

A site investigation was performed in September 2011 by Hernandez (2011), which consisted of two 102 mm-diameter borings located within the building footprint, extending 12 and 7 m below the ground surface. At selected intervals, disturbed samples were obtained by driving split-spoon with a 622.75 N hammer falling 762 mm. Penetration resistance measurements were made during driving. Exploration results from both boreholes were similar and showed three prominent strata, and relevant data is shown in Table 3. The thermal conductivity values were measured on the split-spoon samples of soil using a thermal needle, and provide a preliminary estimate of the thermal conductivity of the subsurface strata. The top layer is approximately 1 m thick and consists of sandy fill. Beneath the fill is a very dense 1 m-thick sandy gravelly layer. The bedrock is Dawson-Arkose (sandstone) extending to the maximum depth explored. No groundwater was encountered during the site investigation or foundation installation, so it is assumed to be at a depth greater than 16 m.

## 3.3 Energy Foundation Descriptions

Eight drilled shafts, each 15.2 m deep by 0.61 m diameter, provide the foundation support for the structure, as shown in Figure 1(a). The one-story building could have been constructed with a shallow foundation, so the main purpose of incorporating the deep drilled shafts into the building was to evaluate the thermo-mechanical response of the energy foundations for this research project. Each foundation contains a 0.46-m-diameter steel reinforcing cage that extends the full length of the shaft. The reinforcing cages are composed of six #7 longitudinal bars with #5 radial hoops spaced at 0.3 m on center throughout the length of the cage. The top of the shafts are

spliced into a 0.91 m-deep by 0.61 m-wide grade beam that extends around the perimiter of the building. Each foundation contains a heat exchanger loop consisting of 19 mm-diameter HDPE tubing. At the top of each foundation, (1 meter below grade), the heat exchanger loop is connected with tubing which is routed through the grade beam [Fig. 1(b)] into a manifold within the mechanical room of the building [Fig. 1(c)].

The heat exchange tubing was attached to the inside of the reinforcing cages such that the inlet and outlet tubes were seperated diametrically by at least 90°, which minimizes thermal short circuiting from the inlet to outlet tubes. The reinforcing cages were lifted with a 3-point pick to minimize bending, and the cages were lowered into the hole with a crane and were suspended on wooden beams to ensure that the top of the cage was at the base of the grade beam. A concrete pump truck was used to place high-slump concrete with a compressive strength ($f'_c$) of 21 MPa in the holes following placement of the reinforcing cages. A tremie pipe was used to avoid excessive segragation of the concrete during free-fall. The use of the tremie also minimized the risk of damage to the heat exchanger loops and embedded instrumentation.

Each shaft has either one, two, or three heat exhanger loops configured in different ways, (Figure 2). Foundations 1 through 4 have identical heat exchanger configurations, with two continuous heat exchanger loops attached to the inside of the steel reinforcement cage. Foundation 5 has three individual loops; each having a supply and return line running to the mechanical room; this permits any combination of the loops to be operational in order to evaluate the efficiency of multiple loops in a single foundation. Foundation 6 has three continuous heat exchanger loops with only one supply and return line extending to the manifolds. Foundation 7 contains one loop connected to the interrior of the reinforcing cage. Foundation 8 has a single loop in the center of the foundation to simulate a retrofit where a heat exchanger would be inserted into a corehole bored into an existing foundation. This was constructed with a 100 mm-diameter plastic sleeve in the center of the foundation. After curing, a single heat exchanger loop was inserted into the plastic sleeve and the hole was grouted with sand bentonite grout.

### 3.4 Instrumentation

Instrumentation was incorporated into three of the eight energy foundations to capture the distribution of axial strain and temperature with depth. Foundations 1 and 3 contain six Geokon Model 4200 vibrating wire strain gauges (VWSGs), while Foundation 4 contains twelve, at the depths shown in Figure 4. Foundation 4 has twice the number of gauges to capture detailed strain and temperature distribution. At three locations within Foundation 4, gauges were located at the same depth on opposite sides of the reinforcing gage to gain redundancy in temperature and strain readings and to capture any differential strain measurements across the width of the shaft. All of the gauges were oriented vertically and attached to brackets welded to longitudinal steel reinforcing bars. The sensor cables were routed to the mechanical room where they are connected to the data acquisition system. Temperature variations in the soil surrounding the

energy foundations are monitored using a series of ten Geokon model 3810 thermistor strings that each have six thermistors spaced equally over the same length as the foundation, installed in boreholes that were then backfilled with CETCO high thermal conductivity grout at the locations shown in Figure 1(a). The temperatures around Foundations 3 and 4 are monitored using four thermistor strings each; with additional thermistor strings located beneath the floor slab and outside the building footprint.

### 3.5 Ambient Ground Temperatures and Construction Strains

Seasonal temperature vs. depth in Foundation 4 was recorded at various times over the course of a year [Fig. 2(a)], as were the axial strains [Fig. 2(b)]. The depths in this figure (and other figures) are measured from the bottom of the grade beam, which is 0.91 m below the ground surface. Ground temperatures fluctuate between 5 °C and 16 °C near the surface then becomes relatively stable at a temperature of 9 °C at depths below 4 m. The axial strains measured in July 2012 reflect the impact of concrete curing, with some tensile strains observed near the head of the foundation. Construction of the floor slab, walls, and roof occurred in Fall 2012, reflected in the increase in axial strain at the head of the foundation. The difference in the strain profiles between February 2013 and July 2012 was assumed to be equal to the mechanical strain in the foundation due the majority of the building load. The strain decreases with depth as expected, with a maximum strain corresponding to an axial load of 833 kN. Similar behavior was noted from the temperatures and strains measured in Foundations 1 and 3.

### 3.6 Testing Scheme

A series of thermal response tests were performed on individual and groups of foundations after the building was constructed. Specifically, an 11 kW thermal response test unit was used to circulate and heat a 20% propylene glycol-water mixture through the foundations. The TRT unit is comprised of four heaters, two rated at 2.5 kW and two at 3 kW. A combination of heaters may be activated to achieve a nominal heat input to the heat exchange fluid ranging from 2.5 kW to 11 kW. Fluid properties of the glycol mixture are shown in Table 4. The heated fluid passed into the supply header, circulated through the foundations, and then passed out of return header back to the test unit. The flow rate of each foundation was measured at one instance during the test on each foundation from the pressure/temperature ports (P/T ports) using a differential pressure meter at a fluid temperature of 30 °C. The differential pressure was then used to compute the flow. During the test, the inlet and outlet temperatures of the heat exchanger fluid for each foundation were continuously monitored using pipe plug thermistors installed within ports on the manifold.

A series of seven test stages were performed to investigate the thermal response of various components of the energy foundation system at USAFA, as summarized in Table 5. In each stage, a nominal heat input was selected to avoid heating any foundation component too rapidly. Stage 1 involved heating Foundations 1-4 simultaneously. Since each of these foundations has an

identical loop configuration within the foundation itself, the effects of the horizontal length of tubing required to connect each foundation to the manifold (called 'run-out length') was documented (Murphy et al. 2014). Stage 1 operated for 498 hours with the intent of allowing sufficient time to increase the temperature of the soil surrounding the foundations and to observe the temperature rise in the boreholes 3-10. Stages 2-4 were conducted on Foundations 6-8 individually with a nominal heat input to the fluid of 5 kW and duration of approximately one week for each stage. Stages 5-7 were conducted on Foundation 5, which has 3 individual loops that can be turned on and off at the manifold. Stage 5 operated on only Loop 5A. During stage 6, Loop 5B of was activated while continuing to pass fluid through Loop 5A. In stage 7, all 3 loops in Foundation 5 were switched open so that flow was permitted to pass through all three loops. Stages 5-7 utilized a 2.5 kW heater in the thermal response test unit. The input heat flux was calculated using Eq. 4 for each heat exchanger loop during each stage.

## 4 Thermal Response Test Results

The fluid temperatures vs. elapsed time are shown in Figure 3. The differences in fluid temperatures, $\Delta T$, are also plotted on the right vertical axis for each foundation. In all cases, a relatively rapid rise in temperature was observed in the first 25 hours. At one segment during stage 1, the data acquisition system malfunctioned and is represented by a gap in the data [Figs. 3(a) to 3(d)]. A constant $\Delta T$ value reflects uniform heat input energy into the system, and these conditions prevailed after about 100 hours of testing in each stage. Note that the differential temperature is greater for longer horizontal run-out lengths, indicating that heat exchange occurs in the grade beam and can have an impact on heat exchange performance.

The temperatures of the three instrumented foundations at different depths are shown in Figures 4(a), 4(b), and 4(c). The thermistor at the bottom of each of the foundations showed a substantially lower increase in temperature than in the rest of the foundation. This may be due to denser rock at the toe of the foundation, potential rises in the water table at the time of testing, or due to the geometry of how the heat exchangers were routed to the U-connector at the base of the foundation. After approximately 498 hours of heating, fluid circulation in Foundations 1-4 was stopped and the temperatures in the foundation were monitored during the cooling process. The deeper portions of the foundations cooled more rapidly, as they were not influenced by the warm ambient air temperature at the ground surface. The foundations returned to their original temperatures after approximately 700-1000 hours after the end of heating. Fluctuations in the uppermost thermistors during cooling reflect the impact of the seasonal ground temperature fluctuations.

Foundation heating led to an increase in ground temperatures measured by the thermistor strings. The temperatures measured in Borehole 1, located at a distance of 4.6 meters outside of the building footprint, are shown in Figure 5(a). The temperature fluctuations occur only near the surface and appear to be due to hot weather. The temperatures measured in Borehole 2, located under the building slab in the center of Foundations 1-4, are shown in Figure 5(b). Although

some changes in temperature near the top of the borehole appear to correspond with the increase in surface temperature during the summer, the temperature of the subsurface at the bottom of the borehole experienced an increase in temperature by about 2°C below a depth of 8m likely due to the heating of the subsurface due the operation of Foundations 1-4. After stage 1 ended, the borehole temperature slightly decreased and remained nearly unchanged from 8/15/13 to 9/4/13.

The temperatures measured in Boreholes 3 through 6, which are located at different radial distances from Foundation 4, are shown in Figure 6. The temperatures at 1.2 m from the center of Foundation 4 [Figs. 6(a) and 6(b)] increase more rapidly than those located at 2.4 m from the center of the foundation [Figs 6(c) and 6(d)]. The temperatures under the building slab, were affected less by changes in the surface temperature than those that were not under the building slab. This suggests that the floor slab acts as an insulator. This effect may be enhanced after the heating system in the building is used to maintain a constant temperature within the building envelope.

## 5 Evaluation of Thermo-mechanical Behavior

To evaluate the thermo-mechanical response of the energy foundations, the resonant frequency values, *f,* from the VWSGs during the heating test were first converted into axial strain ε, as follows:

$$\varepsilon = -Gf^2 \qquad \textbf{(5)}$$

where G is the gage factor equal to $3.304 \times 10^{-3}$ and the units of ε are micro-strain. The negative sign follows the geotechnical sign convention where compressive strains are defined as positive. The strain values calculated with Eq. 5 were then converted to thermal strains, as follows:

$$\varepsilon_T = [(\varepsilon_i - \varepsilon_0)B + \alpha_s \Delta T] \qquad \textbf{(6)}$$

where B is the batch calibration factor of 0.975, $\varepsilon_i$ is the measured axial strain at time i, $\varepsilon_0$ is the initial value of axial strain at the end of building construction (i.e., ambient temperature), $\Delta T$ is the change in temperature between the initial reading and the value at time i, and $\alpha_s$ is the coefficient of thermal expansion of the steel wire of –12.2 με/°C. This equation accounts for the elongation of the steel wire in the gage during heating.

The thermal axial strains calculated using Eq. 6 are shown in Figures 7(a), 7(b), and 7(c). As the temperature increases in the foundations, the thermal axial strains become more negative indicating expansion. The fluctuations in thermal axial strain after heating was stopped correlate well with the observed changes in foundation temperature due to the changes in surface temperature. The strain gauges near the top of each instrumented foundation display the greatest variation, as this is the depth range that is subjected to the greatest change in temperature.

Instances in time corresponding to average changes in foundation temperature of 6 °C during heating and cooling were selected to generate thermo-mechanical profiles for each foundation. The profiles of foundation temperature in Figure 8 show that the temperature is relatively constant in the foundation, except for the base of the foundations, and slight variations in the shape of the temperature profile with time are observed in the top of the foundation due to surface temperature effects. The corresponding changes in thermal axial strain are shown in Figure 9. The shapes of the thermal axial strain profiles are relatively consistent for each foundation. A large thermal axial strain at the toe of each foundation was observed even through the change in temperature was not significant. Although this could be due to issues with the temperature measured by the thermistors at these depths, it could also reflect the possibility that the toe of the foundations may be relatively soft. This would be the case if the loose sandstone cuttings were not thoroughly removed from the bottom of the holes during construction. The distributions in thermal axial strain in Figure 9 reflects that soil-structure interaction due to mobilization of side shear resistance leads to a nonlinear distribution in thermal strain with depth, similar to the observations of Laloui et al. (2006) and Bourne-Webb et al. (2009) during the heating portions of their tests.

Profiles of thermal axial stress were calculated using Eq. (2) with a Young's modulus of 30 GPa (Figure 10). If the foundations were completely restrained, the maximum thermal axial stress that could be generated for an increase in temperature of 18 °C is 6.48 MPa. As the strain gage measurements indicate that some strain occurs in the foundations during heating, the thermal axial stresses in the foundations are all lower than this value. The thermal axial stress generally increases with depth for each of the foundations, although the stress appears to decrease below a depth of 11 to 12 m in each of the foundations. As the point of maximum thermal axial stress typically coincides with the point of zero axial displacements, it is possible that the null point in the foundations occurs at a depth of 11 to 12 m below the grade beam. The thermal axial stresses in Foundation 3 were observed to be nearly 1 MPa lower than in the other two foundations. This could be attributed to the lower amount of restraint provided by the corner of the building compared to the center of the grade beam. Further, Foundations 5 and 8 were not heated, so they may provide greater constraint to Foundations 1 and 4 than to Foundation 3. The thermal axial stresses observed in these three foundations are below 33% of the compressive strength of reinforced concrete ($f'_c$). Even if the foundations were fully restrained (i.e., the case where the measured thermal axial strain is close to zero), the maximum thermal axial stress of 6.48 MPa would be less than this limit.

The mobilized side shear stress due to changes in foundation temperature was calculated from the difference in thermal axial stress values at different heights in the soil layer, as follows:

$$f_{s,mob,j} = \frac{\left(\sigma_{T,j} - \sigma_{T,j-1}\right) D}{4\Delta l} \qquad \textbf{(7)}$$

where D is the shaft diameter and $\Delta l$ is the distance between gages. The sign convention for the mobilized side shear stress implies that positive side shear stresses are upward (in the same direction as those mobilized during mechanical loading), while negative side shear stresses are downward (in the opposite direction as those mobilized during mechanical loading). The mobilized side shear stress profiles calculated for the greatest change in temperature of 18 °C for all three foundations are shown in Figure 11. The results indicate that a negative (downward) side shear stress was observed in the upper portion of the foundation, and a positive (upward) side shear stress was observed in the lower portion of the foundation. The point at which the signs of the mobilized side shear stress changes is in the region of the maximum thermal axial stress and corresponds to the position of the null point. The mobilized side shear stress increases with depth as expected, and the absolute value is less than 200 kPa, which is reasonable for a weakly cemented sandstone.

Although the actual displacements of the toe and head of the foundations were not measured, the relative thermal axial displacements to the bottom of the foundations could be calculated by integrating the thermal axial strain profiles, as follows:

$$\delta_{T,i} = \delta_{T,i-1} + \frac{1}{2}(\varepsilon_{T,i-1} + \varepsilon_{T,i})\Delta l \qquad \textbf{(8)}$$

where $\delta_{T,i}$ is the thermal axial displacement at the midpoint between gages, $\varepsilon_{T,i}$ is the thermal axial strain at the location of gage $i$. The profiles of thermal axial displacement for the three foundations suggest that Foundation 3 experienced a greater displacement at the head of the foundation than the other two foundations (Figure 12), likely for similar reasons contributing to the lower thermal axial stress in it. Although the relative displacement at the toe is assumed to be zero for the purposes of calculating the thermal axial displacements, this does not assume that the null point is at the toe. For a rigid, end-bearing foundation, it is expected that the null point should be close to the toe as by definition it should not be able to move downward. If this were the case, then the maximum upward movement of the head would range from -1.3 to -1.7 mm during a change in temperature of about 18 to 19 °C. On the other hand, if loose cuttings are present at the toe, it is possible that the null point would move upward. If the null point is assumed to be at a depth of 11 to 12 m, then the point of zero axial displacement can also be assumed to occur at this depth, shifting the profiles of displacement to the left. In this case, the upward displacement at the foundation head would range from -1.0 to -1.4 mm and the downward displacement at the foundation toe would range from 0.2 to 0.3 mm. If the toe does not move, the maximum upward displacements will lead to an angular distortion $\delta/L_s$, where $\delta$ is the difference in displacements of two adjacent energy foundations and $L_s$ is the horizontal spacing between the foundations, of less than 1/5000. This value is lower than the limit expected to cause architectural damage in the building (Skempton and MacDonald 1956, Bjerrum 1963).

The foundations experienced linear changes in thermal axial strain with changes in temperature [Fig. 13]. During the cooling phase, the strain for each foundation was observed to

393 nearly return to the values that were experienced during the heating portion of the test, further
394 indicating linear elastic behavior of the reinforced concrete. Relatively little hysteresis was
395 observed, indicating that the mobilized side shear resistance during the heating test did not lead
396 to locked-in plastic strains at the interface. The slope of each trend was defined as the mobilized
397 coefficient of thermal expansion, and the profiles of this coefficient with depth are plotted in
398 Figure 13(d). For each foundation, the mobilized coefficient of thermal expansion was less than
399 that of free expansion ($\alpha_c = -12$ με/°C), indicating that side shear resistance and the end restraint
400 boundary conditions prevented the foundation from expanding as much as it possibly could in
401 free-expansion conditions. The lowest value of the mobilized coefficient of thermal expansion in
402 each of the foundations was observed at a depth of 11 to 12 m, consistent with the location of the
403 maximum thermal axial stress. Foundation 3 exhibited slightly greater mobilized coefficients of
404 thermal expansion likely due to the lower amount of restraint provided by the corner of the
405 building.

406 The ranges in stress in Foundations 1, 3, and 4 are consistent with those observed from the
407 other full-scale foundations reported in the literature (Table 1). The change in thermal axial
408 stress with the change in temperature for Foundations 1, 3, and 4 are shown along with published
409 data from the literature in Figure 14. The depth corresponding to the greatest increase of thermal
410 stress within each foundation was used to define the maximum rates of axial stress during
411 heating. The depths shown correspond to the null point of each foundation and show the greatest
412 thermal axial stress rate. Rates of $\sigma_t = 210\Delta T$ to $260\Delta T$ were determined from the results in this
413 study, which are slightly higher than values from Laloui et al. (2006) and Bourne-Webb et al.
414 (2009), but are consistent with those calculated from the results of McCartney and Murphy
415 (2012). This may be due to the greater coefficient of thermal expansion of the reinforced
416 concrete used in this study (-12 με/°C), which is slightly higher than the value of -9.5 με/°C used
417 in the studies of Laloui et al. (2006) and Bourne-Webb et al. (2009).

418 **6 Evaluation of Thermal Behavior**

419 The details of each heating stage and results from the thermal response tests are summarized
420 in Table 6. The measured heat input for each heat exchanger configuration was normalized over
421 the effective length of the energy foundation system element to define the heat flux per unit
422 meter of heat exchanger Q/L. The effective length, L, is defined as the distance from the
423 manifold to the tip of the foundation. The effective length includes the horizontal run-out length
424 of tubing cast in the grade beam in addition to the 15.2 m length of each foundation. The heat
425 exchange rate is used in this study to assess the relative heat exchange behavior of each
426 foundation because of the geometry of the horizontal connection between the energy foundations
427 and the manifold, which does not satisfy the assumptions of the available analytical methods.
428 The values of Q/L range from 24.4 to 108.5 W/m, which are within the range reported by
429 Bourne-Webb (2013). The value of Q/L was found to be highly dependent on the effective length
430 and nominal heat input, with a decrease in Q/L with increasing effective length. The response is

similar to the decrease in heat flux for increasing length to diameter ratios observed by Bourne-Webb (2013).

As the horizontal run-out length is increased, the heat exchange rate is observed to decrease as some heat loss or gain occurs in the grade beam (Murphy et al. 2014). The effect of the horizontal run-out length can be assessed by evaluating the Q/L results from Foundations 1 through 4, as shown in Figure 15. These foundations have different horizontal run-out lengths, but have the same heat exchanger configuration and were tested together in the same test. A linear relationship was used to estimate the corrected value of Q/L representing the response of a foundation without the effect of horizontal run-out length, as follows:

$$(\mathrm{Q/L})_{corrected} = \mathrm{Q/L} - \mathrm{m_{HR}} \times \mathrm{H_{RO}} \qquad \textbf{(9)}$$

where $m_{HR}$ is the run-out length correction factor in (W/m)/m, and $H_{RO}$ is the horizontal run-out length in meters. A value of $m_{HR}$ of -1.16 (W/m)/m was obtained from the slope of the line in Figure 15. The corrected values of Q/L are reported in Table 6. After the correction is applied, values of Q/L for Foundations 1 through 4 ranged from 97.9 to 109.4 W/m. The small differences after correction may be due to the slight difference in flow rate through each of the foundations. The correction approach was applied to the other foundations at the site to eliminate the impact of horizontal run-out length to evaluate the thermal properties of the foundation-soil system alone. The results in Table 6 indicate that Foundation 7 had the highest value of Q/L of 132.2 W/m; and it had the longest continuous length of heat exchanger within the foundation. However, Foundations 7 and 8 both have similar high values of Q/L of 120 and 126.9 W/m even though they only have one continuous heat exchanger. It is possible that these tests were not performed for a long-enough duration so that the effect of the heat capacity of the concrete could be overcome (Loveridge and Powrie 2012). The Q/L for Foundation 5 when only loop 5A was included was lower, but this could have been due to the much higher flow rate used in this test. The flow rate decreased when the valves for loops 5B and 5C were opened as flow was distributed amongst the three loops.

The thermal conductivity of the subsurface surrounding the foundations could be assessed using the temperatures of the subsurface measured using the thermistor strings in the boreholes. The temperatures of Foundation 4 and the surrounding subsurface were plotted at different instances in time, as shown in Figure 16(a). The vertical line in this figure denotes the outside limit of the building slab, and the distances are measured from the center of the foundation. As expected, as Foundation 4 heats up, the temperature of the soil also increases. The thermal conductivity as a function of time at a depth of 7.3 m was calculated using the temperatures from Boreholes 4 and 5 using Eq. 3, as shown in Figure 16(b). For greater times, the temperature gradient, dT/dr, between the foundation and adjacent boreholes became steadier, which produced thermal conductivity values that were constant between 400 and 500 hours. Thermal conductivity of the soil near the end of heating in stage 1 was calculated to be 2.0 and 2.3 W/mK for heat flow through the subsurface in the directions of Boreholes 4 and 5, respectively. These

values of thermal conductivity are consistent with the corrected system thermal conductivity values reported by Murphy et al. (2014) using the line source method to analyze the heating response data reported for stage 1, even though the details of the foundation system do not satisfy the assumptions of this analysis.

## 7 Conclusions

A series of thermal response tests were carried out on eight full-scale energy foundations with various heat exchanger configurations after construction in a new building. Three of eight energy foundations were instrumented with embedded strain gauges and thermistors to capture the thermo-mechanical behavior during heating, while the inlet and outlet fluid temperatures were monitored for each of the foundations to capture their thermal response. Relevant conclusions related to the thermo-mechanical behavior of the energy foundations are as follows:

- During heating over a change in temperature of 18 °C, Foundations 1, 3, and 4 experienced a relatively uniform change in temperature with depth.
- The increase in temperature led to expansive thermal axial strains in each foundation that were smaller than the estimated free expansion strain. The maximum strains in each foundation occurred near the top and bottom.
- The location of the maximum compressive thermal axial stress, which ranged from 4.0 to 5.1 MPa, was located between a depth of 11 and 12 m (at a normalized depth of 0.72 to 0.78). The thermal axial strains were used to calculate the thermal axial stresses induced in each foundation during heating.
- The relative displacement between the head and toe of each instrumented foundation was found to increase nonlinearly upwards. If the toe of the foundation was assumed not to move, the upward displacement of the head of the foundation was estimated to range from -1.3 to -1.7 mm for the maximum increase in temperature. However, if the toe of the foundation was assumed to move downward (which would be the case if the hole was not adequately cleaned) and the null point was co-located with the depth of the maximum thermal axial stress, the upward displacement of the head of the foundation was estimated to range from -1.0 to -1.4 mm. In either case, the thermal axial movements are not sufficient to induce structural or aesthetic damage to the building.
- The end restraint boundary conditions were found to play an important role in the thermal axial stress and displacement profiles in the energy foundations. Foundation 3 was located at the corner of the building and had the lowest end restraint at the top compared to Foundations 1 and 4 which are located beneath the middle of the grade beam, especially considering the fact that Foundations 1 and 4 were also expanding during the same test. The lower head stiffness was found to lead to a lower thermal axial stress in Foundation 3, along with a slightly greater displacement.
- The thermal axial strains, stresses, and displacements during cooling were similar to those during heating, indicating linear thermo-elastic behavior. Little hysteresis was observed,

which indicates that permanent thermo-plastic deformations did not occur at the foundation-subsurface interface.

The results from the temperature measured for various system components in each heating stage were analyzed to determine system thermal behavior. Relevant conclusions related to the thermal behavior of the energy foundations are as follows:

- The heat flux ranged from 64.5 to 108.5 W/m for the foundations considering the role of the horizontal run-out length of tubing connecting the foundations to the manifold, although lower values of 34.5 W/m were measured when performing staged heating tests on Foundation 5.
- Heat exchange through the horizontal portion of the loop contributes to the efficiency of heat exchange and may play an important role in the design of the plumbing of energy foundations. After application of a correction factor to consider the effects of the horizontal run-out length, the heat flux ranged from 97.9 to 138.2 W/m, and it was possible to consider the relative impacts of different heat exchange configurations. The foundations with a single heat exchanger loop had relatively high values of heat flux per meter, nearly as high as that of a foundation with 3 continuous heat exchangers. This may be due to the large thermal mass that the single heat exchanger must overcome, leading to a higher Q/L than expected in a long-term test.
- The building slab was observed to lead to an insulating effect that led to more stable temperatures in the subsurface. This issue may become more significant when the temperature of the building is maintained at a constant temperature.
- The temperatures of the subsurface measured using thermistor strings in boreholes surrounding Foundation 4 were used to calculate thermal conductivity of the subsurface. The thermal conductivity at a depth of 7.3 m was observed to range from 2.0 to 2.3 W/mK.

## Acknowledgements

Support from DoD ESTCP project EW-201153 is gratefully acknowledged, as are the contributions of the 819th Air Force RED HORSE Squadron, who provided support for the heating test. The views in the paper are those of the authors alone.

## References

Adam, D. and Markiewicz, R. (2009). "Energy from earth-coupled structures, foundations, tunnels and sewers." Géotechnique. 59(3), 229-236.

Amatya, B.L., Soga, K., Bourne-Webb, P.J., Amis, T. and Laloui, L. (2012). "Thermo-mechanical behaviour of energy piles." Géotechnique. 62(6), 503–519.

Bjerrum, L. (1963). "Allowable settlement of structures." Proc., European Conf. on Soil Mech. and Found. Engr., Wiesbaden, Germany, Vol. 3, pp. 135- 137.

541 Bourne-Webb, P.J., Amatya, B., Soga, K., Amis, T., Davidson, C. and Payne, P. (2009). "Energy
542 pile test at Lambeth College, London: Geotechnical and thermodynamic aspects of pile
543 response to heat cycles." Géotechnique. 59(3), 237-248.
544 Bourne-Webb, P. (2013). "An overview of observed thermal and thermo-mechanical response of
545 piled energy foundations." European Geothermal Congress. Pisa, Italy. 8 pg.
546 Brandl, H. (2006). "Energy foundations and other thermo-active ground structures."
547 Géotechnique. 56(2), 81-122.
548 Brettmann, T. and Amis, T. (2011). "Thermal conductivity evaluation of a pile group using
549 geothermal energy piles." GeoFrontiers 2012. Dallas, TX. 10 pg.
550 Energy Information Administration (EIA). (2008). Annual Energy Review. Report No.
551 DOE/EIA-0384(2008).
552 Gao, J., Zhang, X., Liu, J., Li, K. and Yang, J. (2008). "Numerical and experimental assessment
553 of thermal performance of vertical energy piles: an application." Applied Energy. 85(10),
554 901-910.
555 Hamada, Y., Saitoh, H., Nakamura, M., Kubota, H. & Ochifuji, K. (2007). "Field performance of
556 an energy pile system for space heating." Energy and Buildings. 39(5), 517–524.
557 Hughes, P.J. (2008). Geothermal (Ground-Source) Heat Pumps: Market Status, Barriers to
558 Adoption, and Actions to Overcome Barriers. Oak Ridge Nat. Lab. Report ORNL-2008/232.
559 Kavanaugh, S., Rafferty, K., and Geshwiler, M. (1997). Ground-Source Heat Pumps – Design of
560 Geothermal Systems for Commercial and Industrial Buildings. ASHRAE. 167 pp.
561 Laloui, L., Nuth, M., and Vulliet, L. (2006). "Experimental and numerical investigations of the
562 behaviour of a heat exchanger pile." International Journal for Numerical and Analytical
563 Methods in Geomechanics 30, 763–781.
564 Laloui, N. and Nuth, M. (2006). "Numerical modeling of some features of heat exchanger pile."
565 Foundation Analysis and Design: Innovative Methods (GSP 153). ASCE. Reston, VA. pp.
566 189-195.
567 Lennon, D.J., Watt, E., and Suckling, T.P. (2009). "Energy piles in Scotland." Proceedings of the
568 5th International Conference on Deep Foundations on Bored and Auger Piles, Frankfurt (Van
569 Impe, W.F. and Van Impe, P.O. (eds)). Taylor and Francis, London, UK.
570 Loveridge, F. and Powrie, W. (2012). "Pile heat exchangers: Thermal behaviour and interactions."
571 Proc. ICE – Geotechnical Engineering. 166(GE2), 178-196.
572 McCartney, J.S. and Murphy, K.D. (2012). "Strain distributions in full-scale energy
573 foundations." DFI Journal. 6(2), 28-36.
574 McCartney, J.S. and Rosenberg, J.E. (2011). "Impact of heat exchange on the axial capacity of
575 thermo-active foundations." GeoFrontiers 2011. Dallas, TX. 10 pg.
576 Mimouni T. and Laloui L. (2013). "Towards a secure basis for the design of geothermal piles."
577 Acta Geotechnica. DOI 10.1007/s11440-013-0245-4. 12 pg.
578 Murphy, K.D. (2013). Evaluation of Thermal and Thermo-mechanical Behavior of Full-scale
579 Energy Foundations. MS Thesis. University of Colorado Boulder.
580 Murphy, K.D., McCartney, J.S., and Henry, K.S. (2014). "Impact of horizontal run-out length on
581 the thermal response of full-scale energy foundations." GeoCongress 2014. Atlanta, GA. 10
582 pg. In press.
583 Ooka, R., Sekine, K., Mutsumi, Y., Yoshiro, S., and SuckHo, H. (2007). "Development of a
584 ground source heat pump system with ground heat exchanger utilizing the cast-in place
585 concrete pile foundations of a building." EcoStock 2007. 8 pp.
586 Ouyang Y., Soga K. and Leung Y.F. (2011). "Numerical back-analysis of energy pile test at

Lambeth College, London." Geo-Frontiers 2011, Dallas, TX. pg. 440-449.
Sanner, B. (2001). "Shallow geothermal energy." GHC Bulletin. June Issue. pg. 19-25.
Sanner, B., Hellstrom, G., Spitler, J., and Gehlin, S.E.A. (2005). "Thermal response test – current status and world-wide application." World Geothermal Congress. Antalya, Turkey.
Skempton, A.W. and MacDonald, D.H. (1956), "Allowable settlement of buildings." Proc. Institute of Civil Engineers. London, Part 3, Vol. 5, pp. 727- 768.
Stewart, M.A. and McCartney, J.S. (2014). "Centrifuge modeling of energy foundations under cyclic heating and cooling." ASCE Journal of Geotechnical and Geoenvironmental Engineering. 11 pg. In press.

**List of Table and Figure Captions:**

**Figure 13. Thermal axial strain with change in foundation temperature at each depth: (a) Foundation 1; (b) Foundation 3; (c) Foundation 4; (d) Mobilized coefficient of thermal expansion with depth for the three instrumented energy foundations.**

**Figure 14. Comparison of the slope of maximum thermal axial stress with change in temperature for the USAFA foundations and those from previous studies.**

**Figure 15. Trends in heat flux per unit meter (Q/L) for Foundations 1 through 4 as a function of horizontal run-out length.**

**Figure 16. (a) Temperatures of Foundation 4 and surrounding soil; (b) Thermal conductivity over the duration of heating from the thermal gradient between the foundation and Boreholes 4 and 5.**

**Table 1. Results of previous studies on thermo-mechanical behavior of energy foundations.**

| Case | Laloui et al. (2006) | Bourne-Webb et al. (2009) | McCartney and Murphy (2012); Murphy (2013) |
|---|---|---|---|
| Site stratigraphy | Alluvial soil, sand and gravel, founded in soft sandstone, groundwater table near surface | Granular fill and sand, founded in stiff fissured silty clay, groundwater table at a depth of 3 m | Urban fill, sand and gravel, founded in shale, locations of perched groundwater |
| Load mechanism at foundation head | Free expansion, building dead load | Load frame | Building dead load |
| Foundation diameter (m) | 0.88 | 0.56 | 0.91 |
| Foundation length (m) | 25.8 | 23 | 14.8 (A), 13.4 (B) |
| Mechanical load during heating test(s) (kN) | 0, 1300 | 1200 | 3840 (A), 3640 (B) |
| Range of $\Delta T$ (°C) | +20.9, +13.4 | -19.0 to +29.4 | -5.0 to +14.0 |
| Depth of minimum thermal axial strain during heating (m) | 21.0 | 17.0 | 11.6 |
| Minimum/maximum thermal axial stress (MPa) | 2.1 | -0.8 to 1.9 | -1.0 to 5.0 |
| Maximum increase in thermal axial stress with temperature (kPa/°C) | 104 | 192 | 260 |
| Range in head displacements (negative is upward) (mm) | -4.2, not measured | 4.0 to -2.0 | 0.8 to -1.6 |

651 **Table 2. Summary of TRT results from previous studies.**

| Case | Hamada et al. (2007) | Ooka et al. (2007) | Gao et al. (2008) | Lennon et al. (2009) | Brettmann and Amis (2011) |
|---|---|---|---|---|---|
| **Foundation type** | 26×D.P. | 2×D.S. | 1×D.S. | 4×D.P. | 3×A.C.I.P. |
| **Foundation length (m)** | 9 | 20 | 25 | 12-17 | 18.3 |
| **Foundation diameter (mm)** | 300 (square) | 1500 | 600 | 244 (round), 270 (square) | 300-450 |
| **# Heat exchanger loops** | 1,2, Indirect/ Direct Pipe | 8 | 1-3 | 1 | 2 |
| **TRT analysis method** | N/A | N/A | Num. Method | Line Source | Line Source |
| **Thermal conductivity (W/mK)** | N/A | N/A | 5.8-6.0 | 2.4-2.6 | 2.5-2.6 |
| **Heat exchange rate (W/m)** | 54-69 (ext.) | 100-120 (rej.) 44-52 (ext.) | 57-108 (rej.) | N/A | 73-80 (rej.) |

652 ***D.S.: Drilled shaft, A.C.I.P.: Auger cast in place pile, D.P.: Driven Pile**
653 **** Rej.: Heat rejection into foundation, Ext.: Heat extraction from foundation**
654

655 **Table 3: Summary of stratigraphy encountered during subsurface exploration at USAFA.**

| Layer | Depth to bottom of stratum (m) | Material encountered | Gravimetric water content (%) | Dry unit weight (kN/m$^3$) | SPT N-Value (blows/300 mm) | Thermal Conductivity (W/mK) |
|---|---|---|---|---|---|---|
| 1 | 1 | Sandy fill w/ silt, gravel | 5 | 18.4 | 70 | 1.118 |
| 2 | 2 | Dense sands, silt, gravel | 7 | 19.2 | 85 | 0.785 |
| 3 | 12+ | Sandstone | N/A | N/A | 50/25.4 mm | 1.233 |

656

657 **Table 4. Heat exchange fluid properties.**

| Water to propylene glycol ratio | Molar heat capacity (J/molK) | Molecular weight (g/mol) | Specific heat capacity (J/kgK) | Fluid density (g/ml) |
|---|---|---|---|---|
| 5:1 | 98 | 30 | 3267 | 1.008 |

658

659 **Table 5. Summary of thermal response testing stages and heat input details.**

| **Testing stage** | **Foundation** | **Testing dates** | **Approximate duration (hours)** | **Nominal heat flux applied (kW)** | **Measured heat flux Q (kW)** |
|---|---|---|---|---|---|
| 1 | 1<br>2<br>3<br>4 | 6/18/13 – 7/9/13 | 498 | 11.0 | 3.133<br>2.696<br>2.180<br>2.081 |
| 2 | 6 | 7/11/13-7/18/13 | 175 | 5.0 | 4.534 |
| 3 | 7 | 7/18/13-7/25/13 | 167 | 5.0 | 4.431 |
| 4 | 8 | 7/25/13-8/1/13 | 165 | 5.0 | 4.075 |
| 5 | 5A | 8/1/13-8/5/13 | 119 | 2.5 | 2.285 |
| 6 | 5A<br>5B | 8/5/13-8/28/13 | 530 | 2.5 | 1.164<br>1.150 |
| 7 | 5A<br>5B<br>5C | 8/28/13-9/4/13 | 163 | 2.5 | 0.797<br>0.803<br>1.201 |

660

661

662 **Table 6: Summary of results from thermal response testing for each stage (Note: all**
663 **foundations have a length of 15.2 m).**

| Testing stage | Foundation | Heat exchanger configuration | Effective length, L (m) | Flow rate (ml/s) | Average $\Delta T_{fluid}$ (°C) | Measured heat flux, Q (W) | Q/L (W/m) | Corrected Q/L (W/m) |
|---|---|---|---|---|---|---|---|---|
| 1 | 1 | 2 loops | 42.6 | 108 | 8.8 | 3133 | 73.5 | 105.2 |
| | 2 | | 33.5 | 119 | 6.9 | 2696 | 80.5 | 101.6 |
| | 3 | | 21.3 | 137 | 4.8 | 2180 | 102.3 | 109.4 |
| | 4 | | 23.6 | 106 | 6.0 | 2081 | 88.2 | 97.9 |
| 2 | 6 | 3 loops | 41.8 | 144 | 4.8 | 4534 | 108.5 | 139.2 |
| 3 | 7 | 1 loop | 54.0 | 108 | 4.5 | 4431 | 82.1 | 126.9 |
| 4 | 8 | 1 loop in center | 63.1 | 126 | 3.9 | 4075 | 64.6 | 120.0 |
| 5 | 5A | 1 loop | 32.7 | 347 | 2.0 | 2285 | 69.9 | 90.1 |
| 6 | 5A | 1 loop | 32.7 | 226 | 1.6 | 1164 | 35.6 | 55.8 |
| | 5B | | | 226 | 1.6 | 1150 | 35.2 | 55.4 |
| 7 | 5A | 1 loop | 32.7 | 189 | 1.3 | 797 | 24.4 | 44.6 |
| | 5B | | | 189 | 1.3 | 803 | 24.6 | 44.8 |
| | 5C | | | 189 | 1.9 | 1201 | 36.7 | 56.9 |

664

665

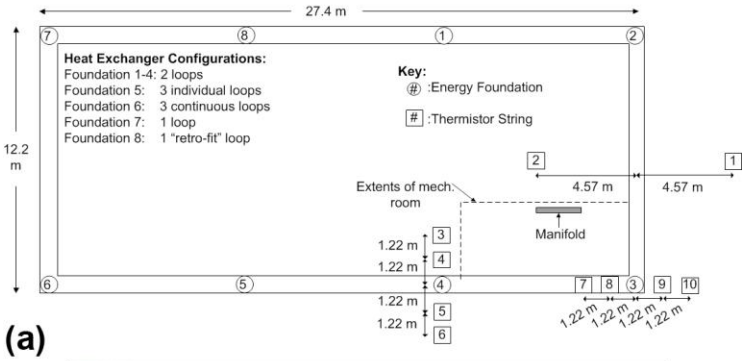


(a)

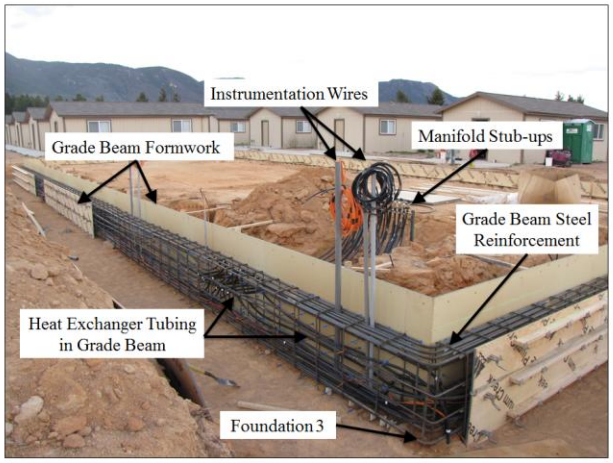


(b)

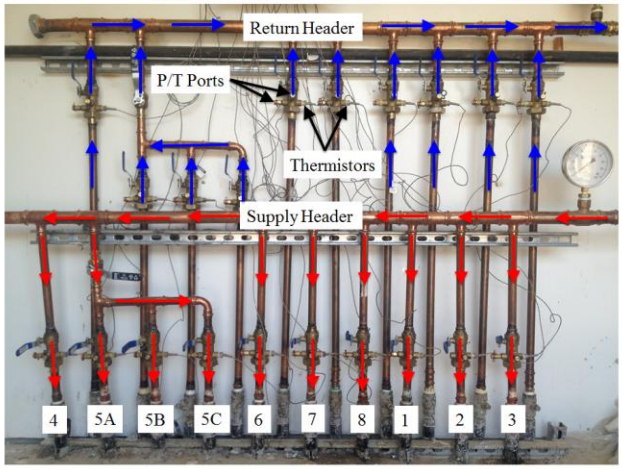


(c)

**Figure 1. (a) Plan view of the building with the locations of the different energy foundations; (b) Heat exchanger tubing configuration in grade beam prior to concrete placement; (c) Manifold detail prior to installation of insulation.**

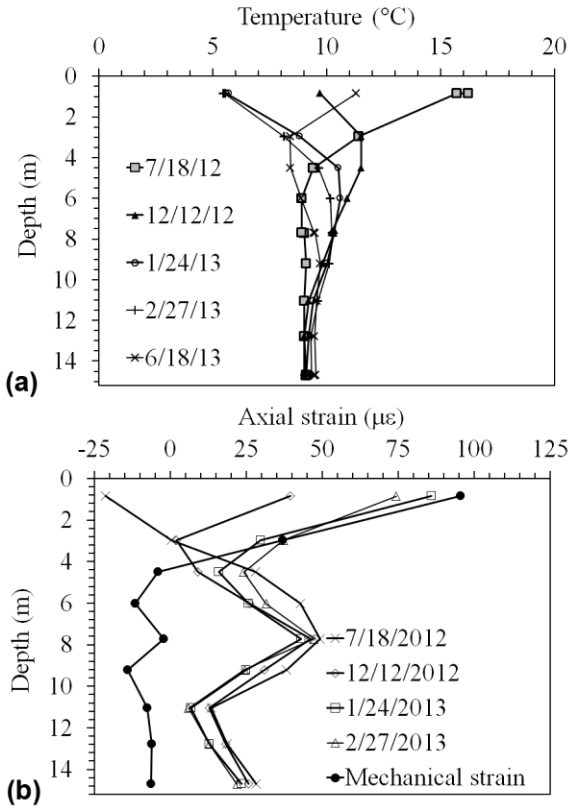


670

671 **Figure 2. Measurements from Foundation 4 during building construction: (a) Profile of**
672 **seasonal temperature variations; (b) Profiles of axial strain during foundation curing**
673 **and building loading, with strains due to mechanical loading.**

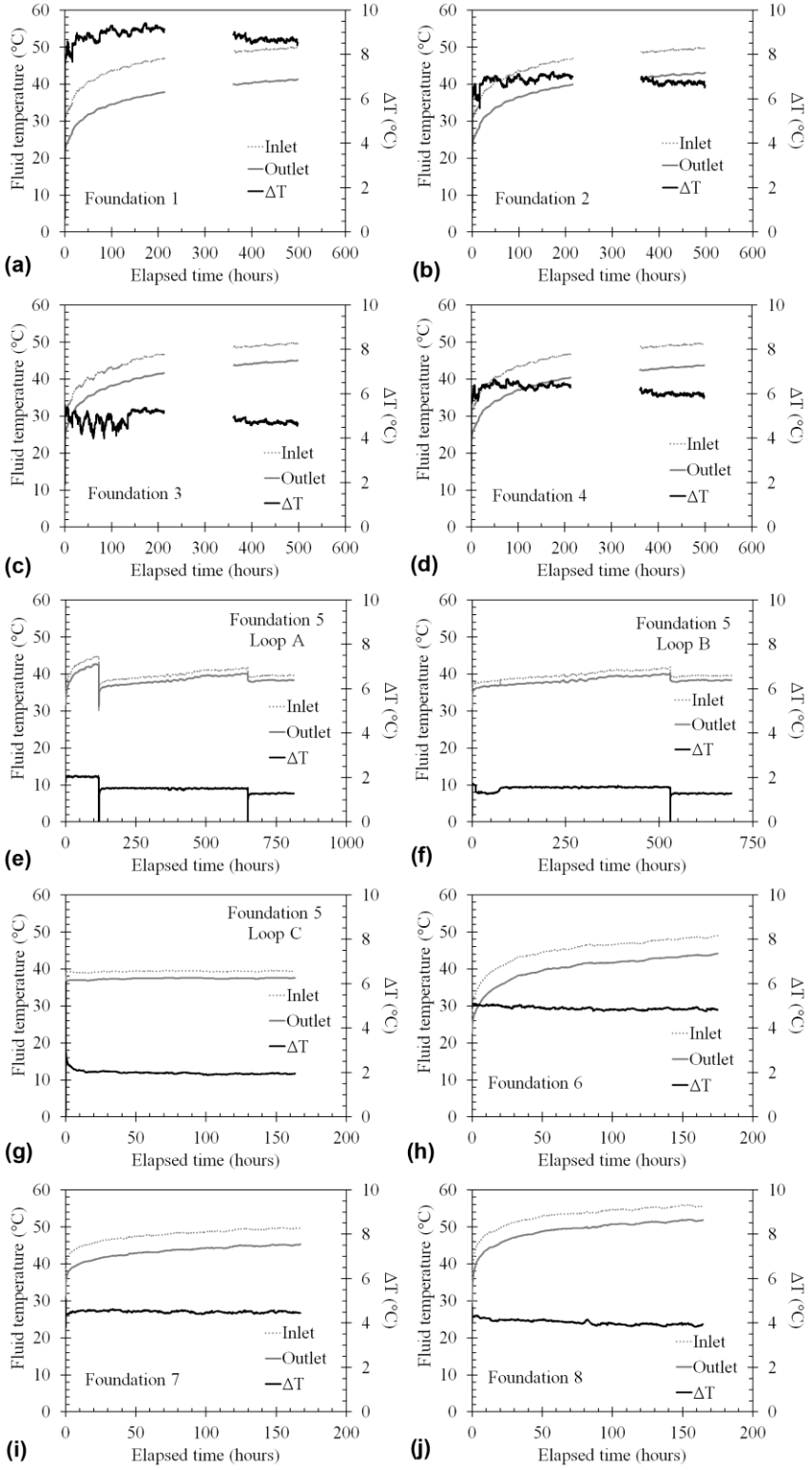


**Figure 3. Fluid temperatures during thermal response testing on Foundations: (a) 1 (Stage 1); (b) 2 (Stage 1); (c) 3 (Stage 1); (d) 4 (stage 1); (e) 5, Loop A (stage 5,6,7); (f) 5, Loop B (Stage 6,7); (g) 5, Loop C (Stage 7); (h) 6 (Stage 2); (i) 7 (Stage 3); (j) 8 (Stage 4).**

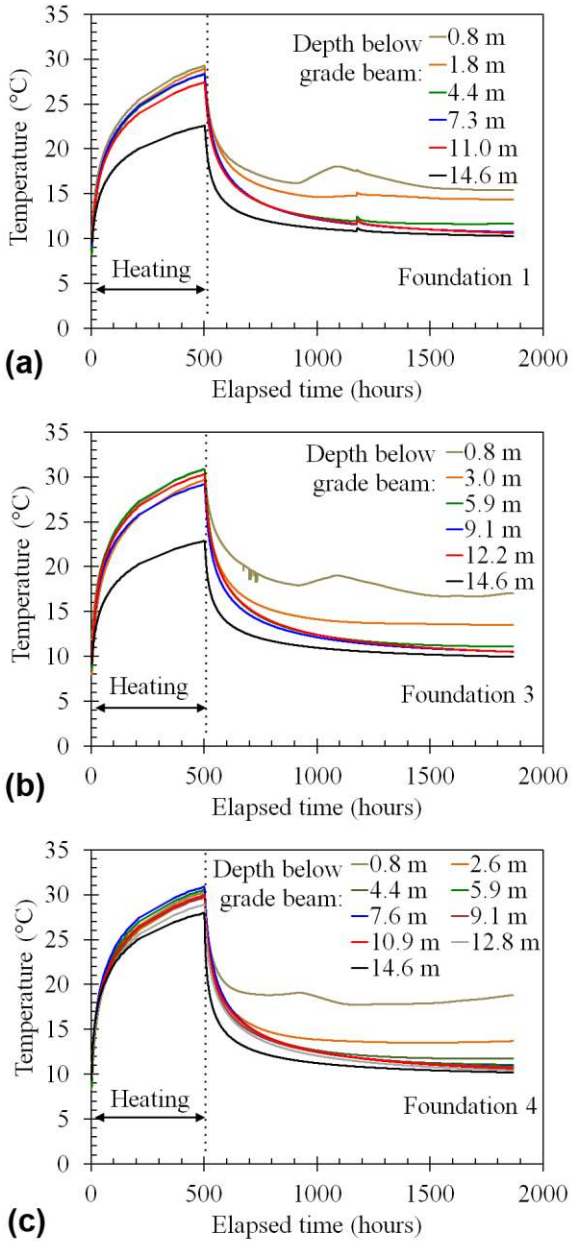


**Figure 4. Foundation temperatures during thermal response testing. (a) Foundation 1; (b) Foundation 3; (c) Foundation 4.**

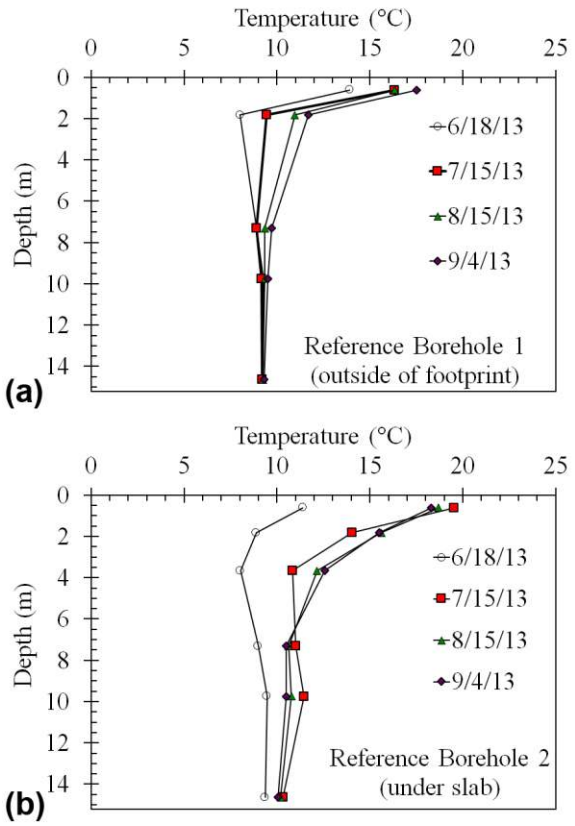


**Figure 5. Temperatures of the subsurface during thermal response testing: (a) Reference Borehole 1; (b) Reference Borehole 2.**

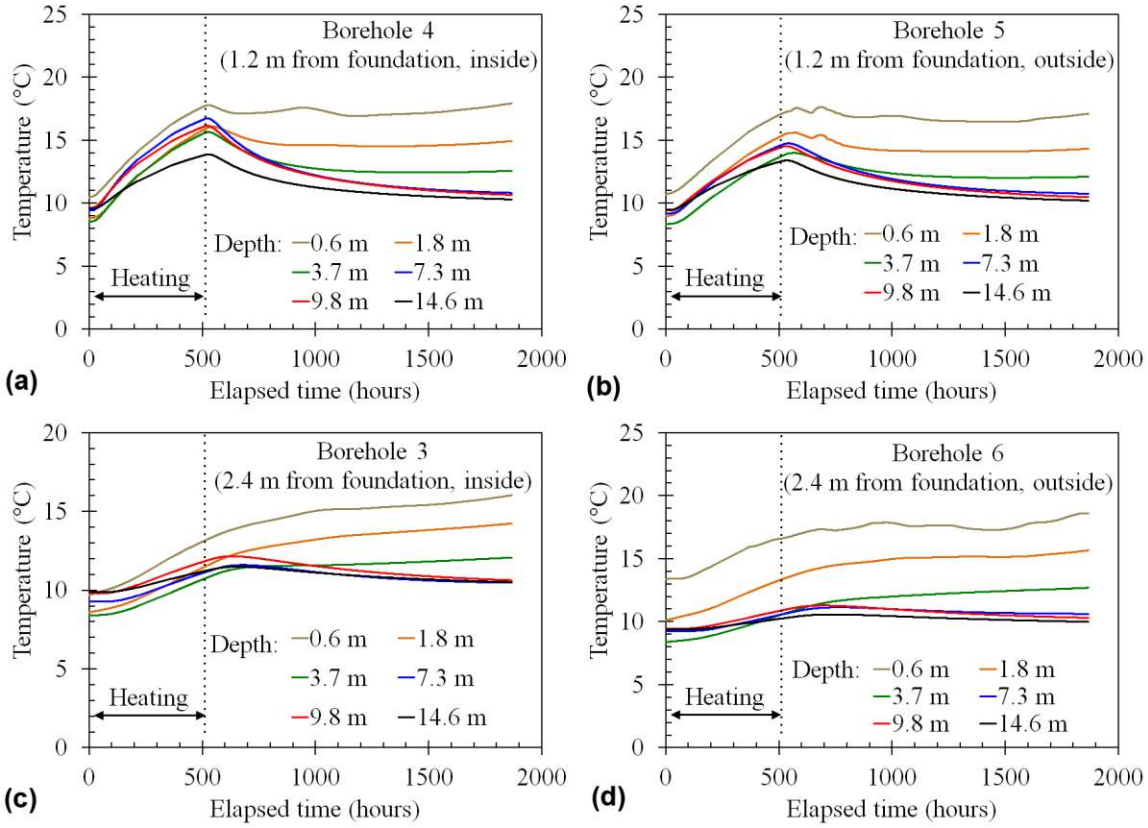


**Figure 6. Subsurface temperatures surrounding the foundations during thermal response testing: (a) Borehole 4; (b) Borehole 5; (c) Borehole 3; (d) Borehole 6**

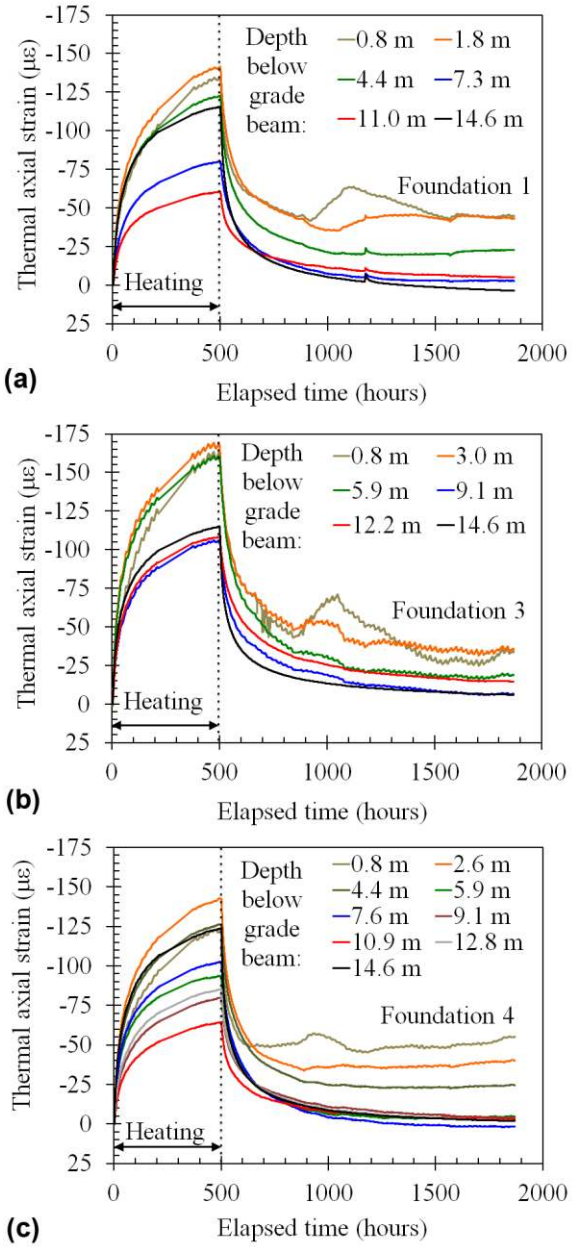


**Figure 7: Time series of thermal axial strains during thermal response testing and subsequent cooling: (a) Foundation 1; (b) Foundation 3; (c) Foundation 4**

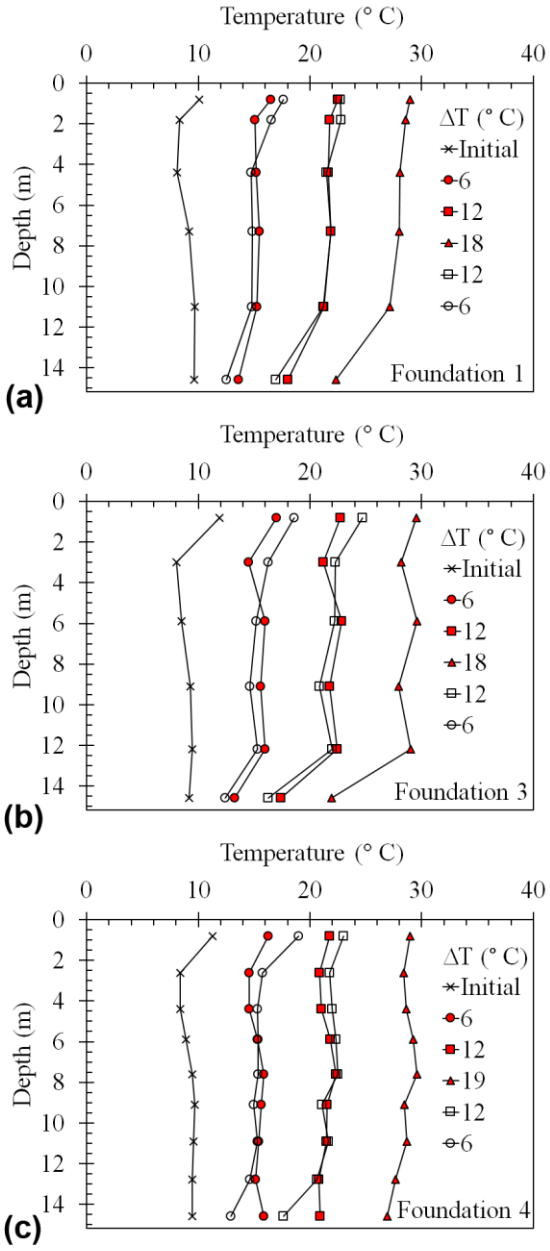


**Figure 8: Profiles of temperature for different average changes in foundation temperature during heating (red) and cooling (open): (a) Foundation 1; (b) Foundation 3; (c) Foundation 4**

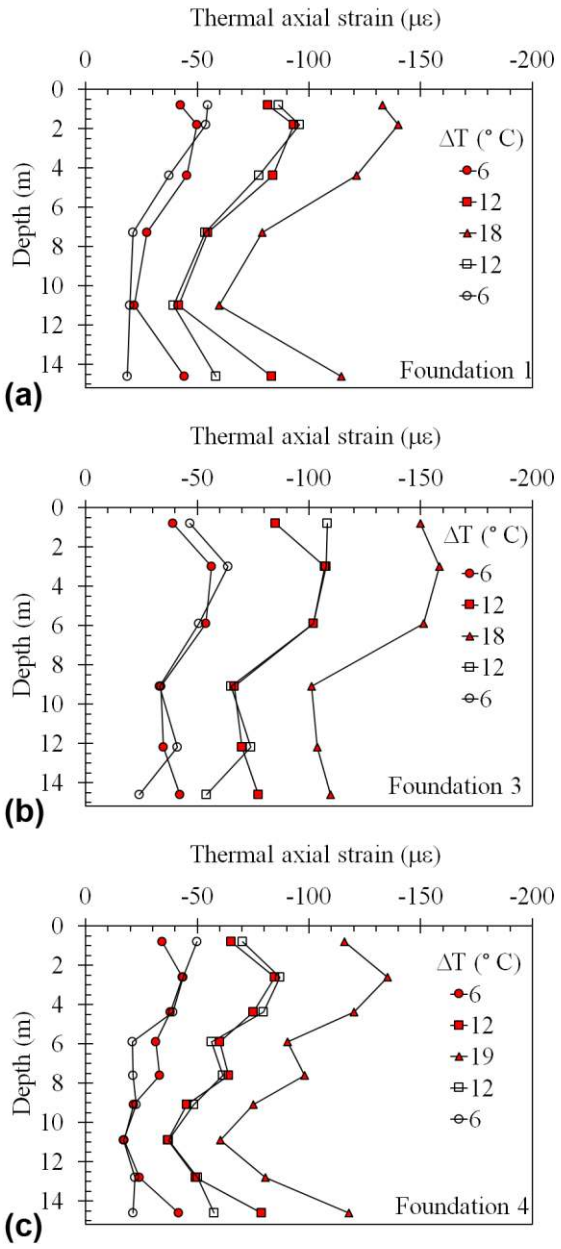


**Figure 9: Profiles of thermal axial strain for different average changes in foundation temperature during heating (red) and cooling (open): (a) Foundation 1; (b) Foundation 3; (c) Foundation 4**

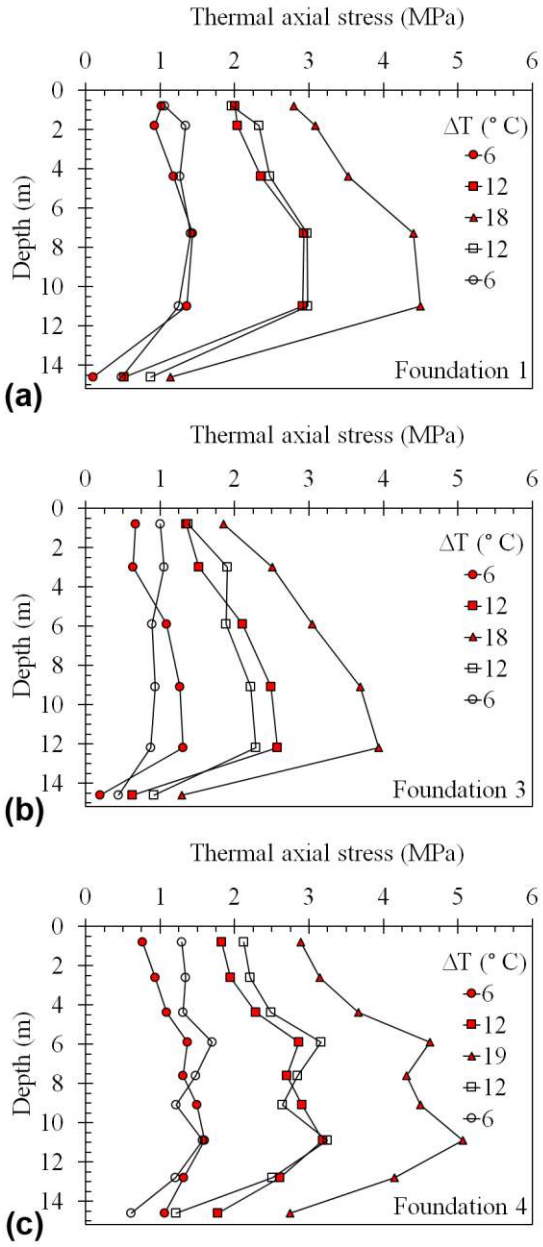


**Figure 10: Profiles of thermal axial stress for different average changes in foundation temperature during heating (red) and cooling (open): (a) Foundation 1; (b) Foundation 3; (c) Foundation 4**

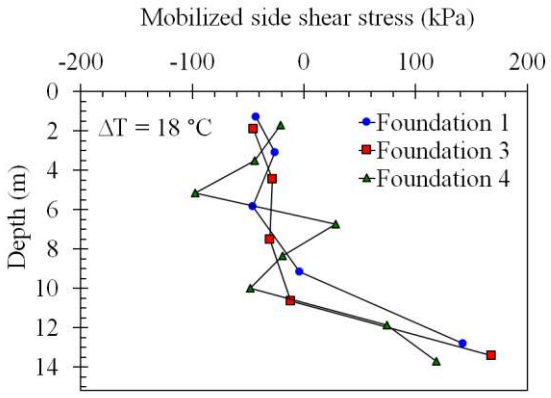


703

704 **Figure 11: Profiles of mobilized side shear for a change in temperature of 18 °C for**
705 **Foundations 1, 3, and 4**

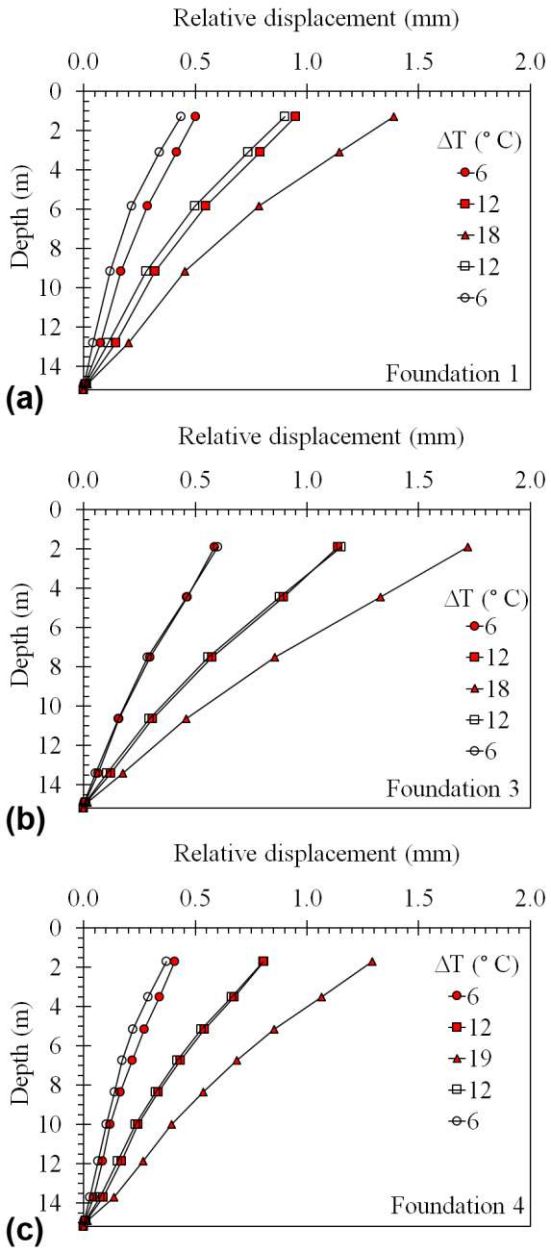


**Figure 12: Profiles of thermal axial displacement for different average changes in foundation temperature during heating (red) and cooling (open): (a) Foundation 1; (b) Foundation 3; (c) Foundation 4**

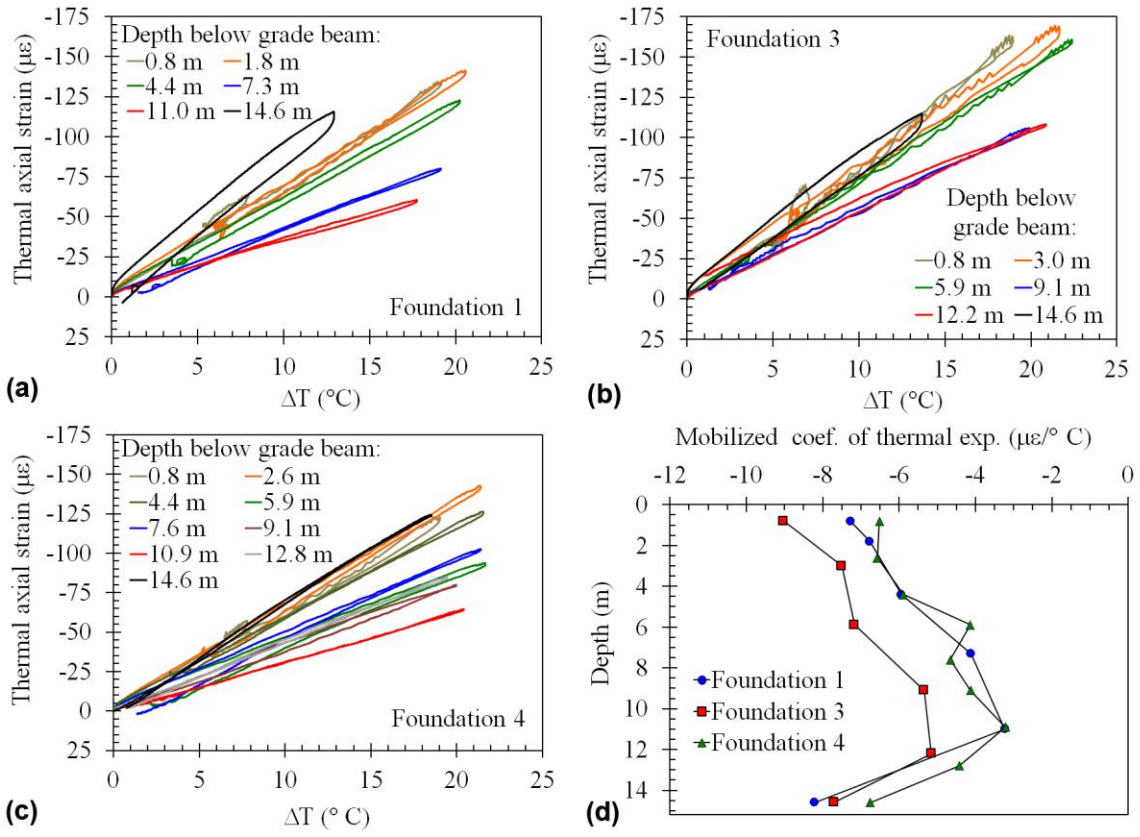


**Figure 13. Thermal axial strain with change in foundation temperature at each depth: (a) Foundation 1; (b) Foundation 3; (c) Foundation 4; (d) Mobilized coefficient of thermal expansion with depth for the three instrumented energy foundations.**

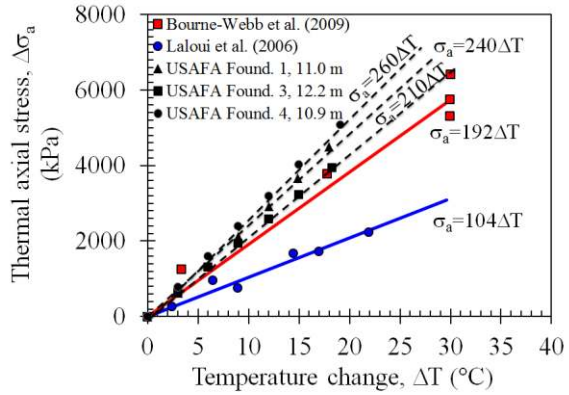


**Figure 14. Comparison of the slope of maximum thermal axial stress with change in temperature for the USAFA foundations and those from previous studies.**

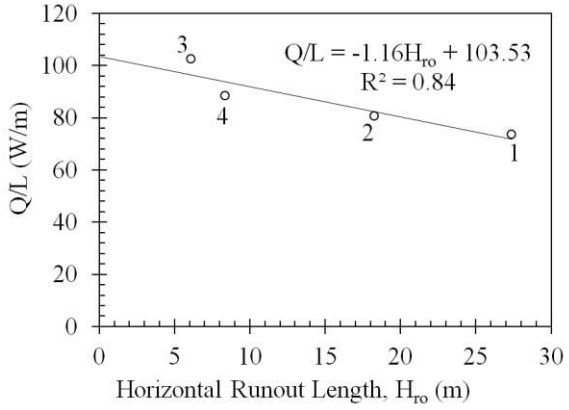


720

721 **Figure 15. Trends in heat flux per unit meter (Q/L) for Foundations 1 through 4 as a**
722 **function of horizontal run-out length.**

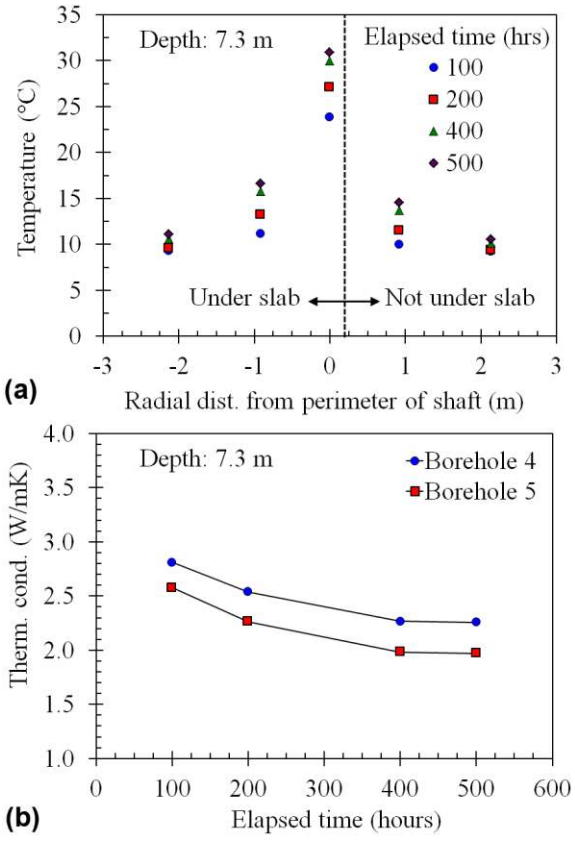


723

724 **Figure 16. (a) Temperatures of Foundation 4 and surrounding soil; (b) Thermal**
725 **conductivity over the duration of heating from the thermal gradient between the**
726 **foundation and Boreholes 4 and 5.**

727